LASER & PHOTONICS REVIEWS
www.lpr-journal.org

Toward Arbitrary Spin-Orbit Flat Optics Via Structured Geometric Phase Gratings

Chun-Yu Li, Si-Jia Liu, Bing-Shi Yu, Hai-Jun Wu, Carmelo Rosales-Guzmán, Yijie Shen, Peng Chen, Zhi-Han Zhu,* and Yan-Qing Lu**

Reciprocal spin-orbit coupling (SOC) via geometric phase with flat optics provides a promising platform for shaping and controlling paraxial structured light. Current devices, from the pioneering q-plates to the recent J-plates, provide only spin-dependent wavefront modulation without amplitude control. However, achieving control over all the spatial dimensions of paraxial SOC states requires spin-dependent control of corresponding complex amplitude, which remains challenging for flat optics. Here, to address this issue, a new type of flat-optics elements termed structured geometric phase gratings is presented, that is capable of conjugated complex-amplitude control for orthogonal input circular polarizations. By using a microstructured liquid crystal photoalignment technique, a series of flat-optics elements is engineered and their excellent precision in arbitrary SOC control is shown. This principle unlocks the full-field control of paraxial structured light via flat optics, providing a promising way to develop an information exchange and processing units for general photonic SOC states, as well as extra-/intracavity mode convertors for high-precision laser beam shaping.

1. Introduction

Recent advances in structured vectorial paraxial beams with tunable spatially-varying amplitude, phase, and state of polarization (SoP) are continually revealing a variety of exotic structured photonic states and unexpected phenomena.[1–4] These vector paraxial modes were discovered in the early years of laser physics but became an active topic only in this century.[5] The mechanism behind the exotic beam structure of vector modes has become widely known only in the last 2 decades, after people became aware of paraxial orbital angular momentum (OAM).[6,7] More precisely, vector modes a nonseparable superposition between the SoP and spatial structure of light, which can also be interpreted as spin-orbit coupling (SOC) in light beams, and the modes are therefore also known as paraxial SOC states, especially in the quantum context.[8–10] Crucially, this mechanism has provided the basis on how to shape and control the SOC states, that is, spin-dependent spatial light modulation. Along this line, there are two feasible approaches: the first one relies on the use of a traditional polarization interferometer, very often comprising a digital spatial light modulator,[11,12] while the other is to exploit the geometric phase, through photonic SOC devices based on delicate flat optics.[13] The former can fully control the spatiotemporal structure of light in a dynamic and flexible way but has a complex, bulky, and inefficient configuration. The latter, owing to its low cost, integrability, and versatility, is gaining increasing attention and popularity in a rapidly developing field.[14,15]

The geometric phase referred to here originates from the slow transformation of the SoP, also known as the Pancharatnam–Berry phase, and its retardance depends on the geometric path on the Poincaré sphere.[16–18] This principle provides a new paradigm for building wavefront-shaping platforms, that is, exploiting the 2D geometric phase resulting from a spatially varied SoP transformation. Specifically, imagine if we pass a beam through a flat element with spatial-variant birefringence, such as microstructured liquid crystals (LCs) or dielectric metasurfaces;[14,15] beyond enabling a point-by-point SoP transformation in the transverse plane, a wavefront modulation with SoP switchable behavior will be achieved. Notably, current SOC devices, from the original LC q-plates to recent metasurface J-plates,[19,20] provide only spatial light modulation of the phase with SoP-switchable behavior. The absence of amplitude control greatly limits the range of SOC

C.-Y. Li, B.-S. Yu, H.-J. Wu, C. Rosales-Guzmán, Z.-H. Zhu
Wang Da-Heng Center, HLJ Key Laboratory of Quantum Control
Harbin University of Science and Technology
Harbin 150080, China
E-mail: zhuzhihan@hrbust.edu.cn

S.-J. Liu, P. Chen, Y.-Q. Lu
National Laboratory of Solid State Microstructures
Key Laboratory of Intelligent Optical Sensing and Manipulation
and College of Engineering and Applied Sciences
Nanjing University
Nanjing 210093, China
E-mail: chenpeng@nju.edu.cn; yqlu@nju.edu.cn

C. Rosales-Guzmán
Centro de Investigaciones en Óptica
A.C., Loma del Bosque 115, Colonia Lomas del campestre, Gto., León 37150, Mexico

Y. Shen
Optoelectronics Research Centre & Centre for Photonic Metamaterials
University of Southampton
Southampton SO17 1BJ, UK

The ORCID identification number(s) for the author(s) of this article can be found under https://doi.org/10.1002/lpor.202200800

DOI: 10.1002/lpor.202200800

achievable states. To illustrate this, we take cylindrical vector (CV) polarized modes (also called vector vortex beams) as an example, which have been considered of paramount importance in applications, such as, high-dimensional communication, remote sensing, microscopy, to mention a few.[21–28] Their modal constitution exhibits "typical" SOC states, that is, a superposition of two conjugate (opposite topological charge) OAM modes with orthogonal circular polarization. Remarkably, CV modes obtained via q-plates are not eigenmodes of free space; and therefore, upon propagation, they give rise to the so-called hyper-geometric Gauss (HyGG) beams.[29] In contrast to propagation of invariant Laguerre–Gauss (LG) modes, their pattern exhibits ripple-like motion upon propagation owing to their undefined amplitude structure.[30] This issue creates difficulties in SOC state manipulation and transmission, but more importantly, it limits the exploitation of all the spatial dimensions of structured light. Without amplitude control, it is impossible to access the radial degree-of-freedom of LG and associated CV modes,[31–35] let alone, to control more general SOC states in other paraxial coordinates.[36–38] That is why q-plate-like flat elements have always been absent from experimental studies involving full spatial dimensions of structured light, and instead, the traditional optical scheme seems to be the only choice of scientists.[39–42]

To control a paraxial SOC state in all its spatial degrees of freedom, spin-dependent complex amplitude modulation provides an essential alternative, but up to now, it has remained elusive with flat optics. In this work, we fill this gap, by putting forward a new type of geometric-phase element termed structured geometric phase grating (SGPG), featuring a spatially-varying grating cycle, depth and orientation. Importantly, this SOC device can structure arbitrarily the complex amplitude of input beams in the ±1st-order of diffractions with a conjugate manner in response to left- and right-circular polarized components, respectively. Such a crucial advance, compared with the present geometric phase elements, unlocks the control of paraxial structured light in all spatial dimensions, and paves the way toward arbitrary SOC conversion via flat optics. To demonstrate this principle, we engineered a series of LC flat elements using a photoalignment technique[15] and experimentally showed their excellent performance in terms of arbitrary SOC control of structured light.

2. Concept and Principle

2.1. Spin-Orbit Coupled States

The term SOC state utilized here refers to the most common family of vectorial paraxial modes constructed by conjugate angular momentum components[43] and can be expressed as a nonseparable superposition of orthogonal circular SoPs $\hat{e}_{\pm}$ (associated to spin angular momentum) and conjugate spatial modes $\psi_{\pm}(\boldsymbol{r}, z)$ carrying opposite OAM:

$$\Psi_{\mathrm{soc}}(\boldsymbol{r}, z) = \sqrt{a}\psi_{+}(\boldsymbol{r}, z)\,\hat{e}_{+} + e^{i\theta}\sqrt{1-a}\psi_{-}(\boldsymbol{r}, z)\,\hat{e}_{-} \tag{1}$$

where $\boldsymbol{r}$ denotes transverse coordinates; $a \in [0, 1]$ is a weighting coefficient that controls the degree of nonseparability (which is maximum for $a = 0.5$), and θ is an intermodal phase. Note that the two OAM-carrying modes $\psi_{\pm}(\boldsymbol{r}, z)$ form a conjugate pair and thus can be expressed as

$$\psi_{\pm}(\boldsymbol{r}, z) = u(\boldsymbol{r}, z)\exp\left[\pm i\nu(\boldsymbol{r}, z)\right], \tag{2}$$

where $u(\boldsymbol{r}, z)$ and $\pm\nu(\boldsymbol{r}, z)$ represent the identical spatial amplitude and conjugate wavefronts of the pair, respectively. All possible vector modes shown in Equation (1) form a tensor parameter space with respect to spin and orbital angular momenta and can be visualized as the surface of a spin-orbit hybrid unit sphere commonly called higher-order Poincaré sphere;[44] although, less rigorous.[45] Here, we call it SOC modal sphere in the following contents. In particular, the SOC state (1) becomes the most common CV mode, as $\psi_{\pm}(\boldsymbol{r}, z)$ are OAM eigenmodes carrying well-defined OAMs, that is, $\pm\ell\hbar$ per photon (ℓ is an integer), such as a pair of conjugate LG, Bessel, or HyGG modes.

Note that state (1) has the same SU(2) algebraic structure as a scalar SoP on the "classical" Poincaré sphere. This indicates that a reciprocal SOC device, if achievable, can realize the interconversion between an arbitrary SOC mode and its corresponding scalar SoP

$$\left(\sqrt{a}\hat{e}_{+} + e^{i\theta}\sqrt{1-a}\hat{e}_{-}\right)\psi_{0}(\boldsymbol{r}, z) \leftrightarrow \Psi_{\mathrm{soc}}(\boldsymbol{r}, z), \tag{3}$$

where $\psi_0(\boldsymbol{r}, z)$ denotes the spatial complex amplitude of the scalar beam and is commonly considered the TEM_{00} mode. In other words, the supposed device can map a SoP on the Poincaré sphere into the same position on an arbitrary desired SOC modal sphere and vice versa, as the example shown in **Figure 1**a. A popular example is the q-plate, used to interconvert a given scalar SoP and its CV-polarized counterpart. The mechanism of this interconversion is realized by imprinting conjugate spiral wavefronts $\exp(\pm i\ell\varphi)$ onto $\hat{e}_{\pm}$ polarization components of the input beam. This widely used spin-dependent phase-only modulation,[13,15,20] although belonging to unitary transformation, fails to define the amplitude structure of $\psi_{\pm}(\boldsymbol{r}, z)$. Namely, the implementation of Equation (3) for general SOC states relies on a reciprocal complex-amplitude transformation $\psi_{\pm}(\boldsymbol{r}, z) \leftrightarrow \psi_0(\boldsymbol{r}, z)$ according to the input SoP. In particular, this arbitrary SOC conversion can work as a controlled gate in the quantum computing system built by photonic SOC states.[46]

2.2. Structured Geometric Phase Gratings

How to build a flat SOC device for structuring arbitrary paraxial vector modes? The task requires that the device, beyond conjugately shaping wavefronts of $\hat{e}_{\pm}$ components, can also structure the amplitude profile directly and preferably without the assistance of other operations, such as polarization filtering. Moreover, the intramodal phase $e^{i\theta}$ should remain unchanged in the conversion. That is, our main focus is to achieve spin-dependent complex amplitude modulation with phase-locking ability.

To achieve this goal, we introduce a new type of geometric-phase element termed the structured geometric phase grating (SGPG) that has spatially-variant grating cycle, depth, and orientation. When guiding a TEM_{00} or $\Psi_{\mathrm{soc}}(\boldsymbol{r}, z)$ mode passing this flat element, the designed mode conjugates $\psi_{\pm}(\boldsymbol{r}, z)$ can

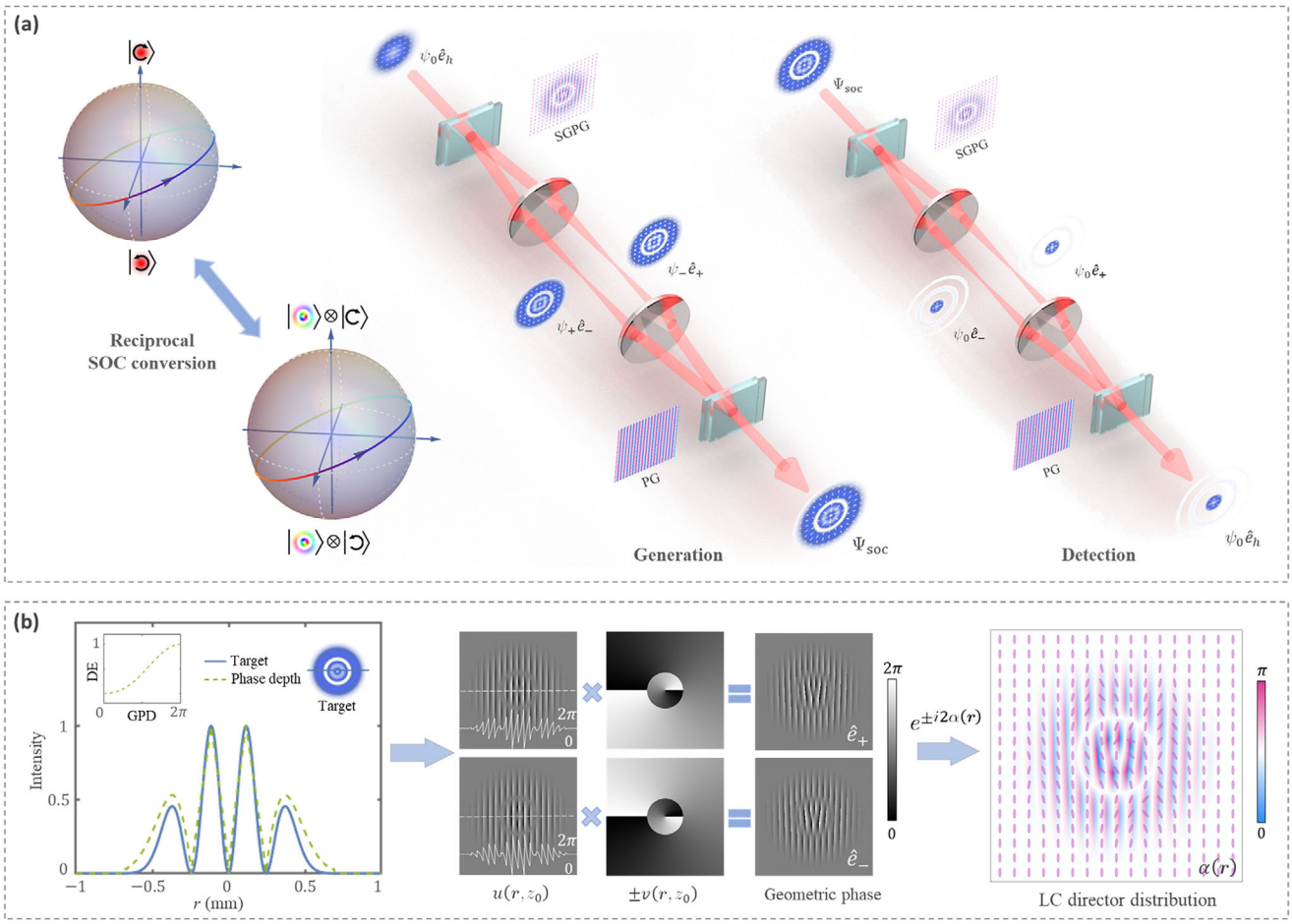

Figure 1. a) Schematic of the reciprocal SOC device based on structured geometric phase gratings (SGPGs) designed for controlling the "example" SOC state composed of $|\mathrm{LG}_{\pm1,1}, \hat{e}_{\pm}\rangle$. b) Inverse design of the SGPG for generating and measuring $|\mathrm{LG}_{\pm1,1}, \hat{e}_{\pm}\rangle$ in ±1st-order diffractions. The left panel shows the target intensity profile to be structured, diffraction efficiency (DE), and the corresponding grating phase depth (GPD) distribution; the middle panel shows the constructed spin-switchable geometric phase; and the right panel shows the LC-director orientations of the designed SGPG.

be generated or measured at the ±1st diffraction orders with opposite circular SoPs. The two diffraction orders can be recombined coherently using a conventional polarizing grating (PG); in this way, the reciprocal SOC device for arbitrary vector modes shown in Equation (3) is realized. Both microstructured LCs and dielectric metasurfaces are good candidates to fabricate SGPGs. Here, we used nematic LC and the photoalignment technique to fabricate all the elements by virtue of their high efficiency, low cost, high reliability, and electro-tunability[47–50]; see Methods for details. These LC elements can be regarded as microstructured half-wave plates with spatially-variant director orientation $\alpha(\boldsymbol{r})$, giving a 2D SoP transformation and associated wavefront modulation $|\hat{e}_{\pm}\rangle \rightarrow \exp[\pm i2\alpha(\boldsymbol{r})]|\hat{e}_{\mp}\rangle$ to circular-polarized components of incident light.

To illustrate the principle specifically, as shown in Figure 1, we choose vector modes constructed by SOC bases $|\mathrm{LG}_{\pm1,1}, \hat{e}_{\pm}\rangle$ as an example to show the inverse design of the geometric-phase elements. That is, in the example, the desired mode conjugates $\psi_{\pm}(\boldsymbol{r}, z)$ were assumed as a dual-ring donut mode pair $\mathrm{LG}_{\pm1,1}$. First, to directly structure the spatial amplitude via geometric phase, we exploit the relation of the grating phase depth (D) to diffractive efficiency (or probability) to control amplitude profiles of light (or photons) in ±1st-order diffractions, given by

$$D\ (\boldsymbol{r}) = 2\pi\left\{1 - \mathrm{sinc}^{-1}\left[u\left(\boldsymbol{r}, z_0\right)\right]\right\}, \tag{4}$$

where $D \in [0, 2\pi]$ and $u(\boldsymbol{r}, z_0)$ denote the amplitude profile (realized via diffractive efficiency control) of desired spatial modes at the $z = 0$ plane. Specifically, in the left panel of Figure 1b, the green dashed line shows a calculated grating phase depth $D(\boldsymbol{r})$ with the blue solid curve as the desired diffractive efficiency (or the beam profile to be shaped) $u^2(\boldsymbol{r})$. Based on this, by integrating the spin-dependent wavefronts $\pm v(\boldsymbol{r}, z_0)\hat{e}_{\pm}$, a pair of geometric phase conjugates used to structure the example mode pairs $\mathrm{LG}_{\pm1,1}$ is obtained, as shown in the middle panel. At last, using the relation between the geometric phase and LC-director orientation $|\hat{e}_{\pm}\rangle \rightarrow \exp[\pm i2\alpha(\boldsymbol{r})]|\hat{e}_{\mp}\rangle$, we obtain the LC-director distribution to fabricate the desired SGPG, as shown in the right panel. This novel geometric-phase element can exactly structure the example SOC bases $|\mathrm{LG}_{\pm1,1}, \hat{e}_{\pm}\rangle$ in ±1st-order diffractions. On this basis, in combination with a 4f-PG polarizing beam combiner, we build a reciprocal SOC device that can map arbitrary scalar SoPs

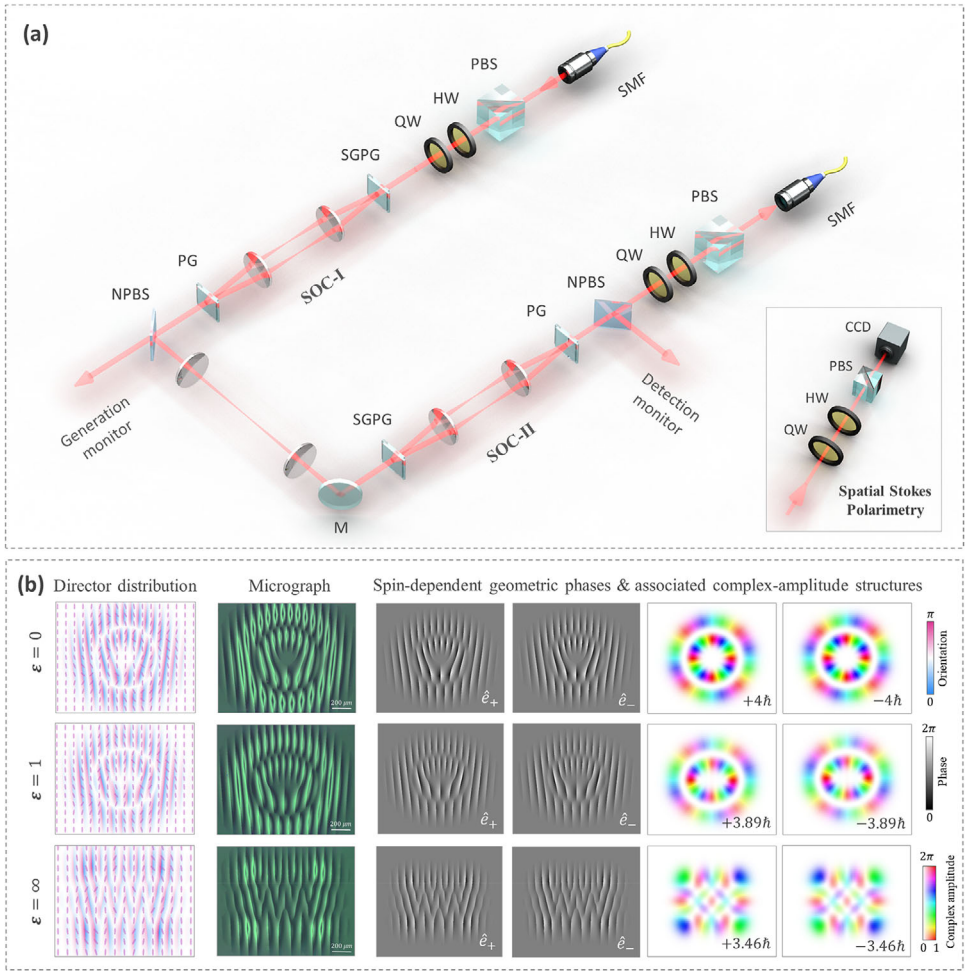

Figure 2. a) Schematic representation of the experimental setup, where the key components are the single-mode fiber (SMF), half-wave plate (HW), quarter-wave plate (QW), polarizing beam splitter (PBS), nonpolarizing beam splitter (NPBS), structured geometric phase grating (SGPG), polarization grating (PG), and camera (CCD). The right-bottom inset shows the constitution of spatial Stokes polarimetry. b) Schematics and characterizations of the SGPG design for generating $|IG^{\pm}_{6,4}, \hat{e}_{\pm}\rangle$ with $\varepsilon = 0,\ 1,$ and ∞, including designed LC director distributions, polarizing micrographs taken at 0 V under crossed polarizers, and target geometric phases (GPs) and complex amplitudes.

into their vector counterpart on the SOC modal sphere defined by $|LG_{\pm1,1}, \hat{e}_{\pm}\rangle$ and vice versa. In addition, there are two noteworthy points. First, incident beams in the generation process are usually in the fundamental Gaussian mode; thus, the corresponding design should contain Gaussian amplitude amendments. Second, the principle of spatial mode detection used here, as well as in other relevant works, is not a strict projective measurement but a spatial autocorrelation.[51–53] More details about the two points are provided in the Supporting Information.

3. Experimental Section

Figure 2a shows the experimental setup used to verify the principle illustrated above. A narrow linewidth laser operating at 780 nm, collimated from a single-mode fiber as a TEM_{00} beam, was used as the initial light source of the experiment. The TEM_{00} beam was first adjusted to the desired polarization using a SoP-control unit consisting of a polarizing beam splitter (PBS) and two wave plates (QW and HW). This scalar polarized TEM_{00} beam was then converted into a corresponding vectorial structured Gaussian beam by passing it through the first SOC convertor (SOC-I), that is, by performing SOC state generation. Then, the generated vector beam was guided into the second SOC convertor (SOC-II), which operated in the detection mode, and was converted back to a corresponding scalar polarized beam. All the LC elements were operated in the half-wave condition by controlling their load voltage (a 1 kHz square-wave signal with a peak-peak voltage of ≈2 V was applied). To match the beam size and divergence in SOC state generation and detection, a 4f-system was placed between the two SOC convertors. Last, another SoP-control unit was used to perform Stokes tomography on the scalar polarized beam output from SOC-II, and projective values (i.e., Stokes parameters) were received by a single-mode fiber. In addition to an in situ measure of the beam structure in SOC state generation and detection operations, spatial Stokes polarimetry was used (see the apparatus in the right-bottom inset in Figure 2a) to monitor polarizing beam patterns sampled from two nonpolarizing beam splitters (NPBSs).

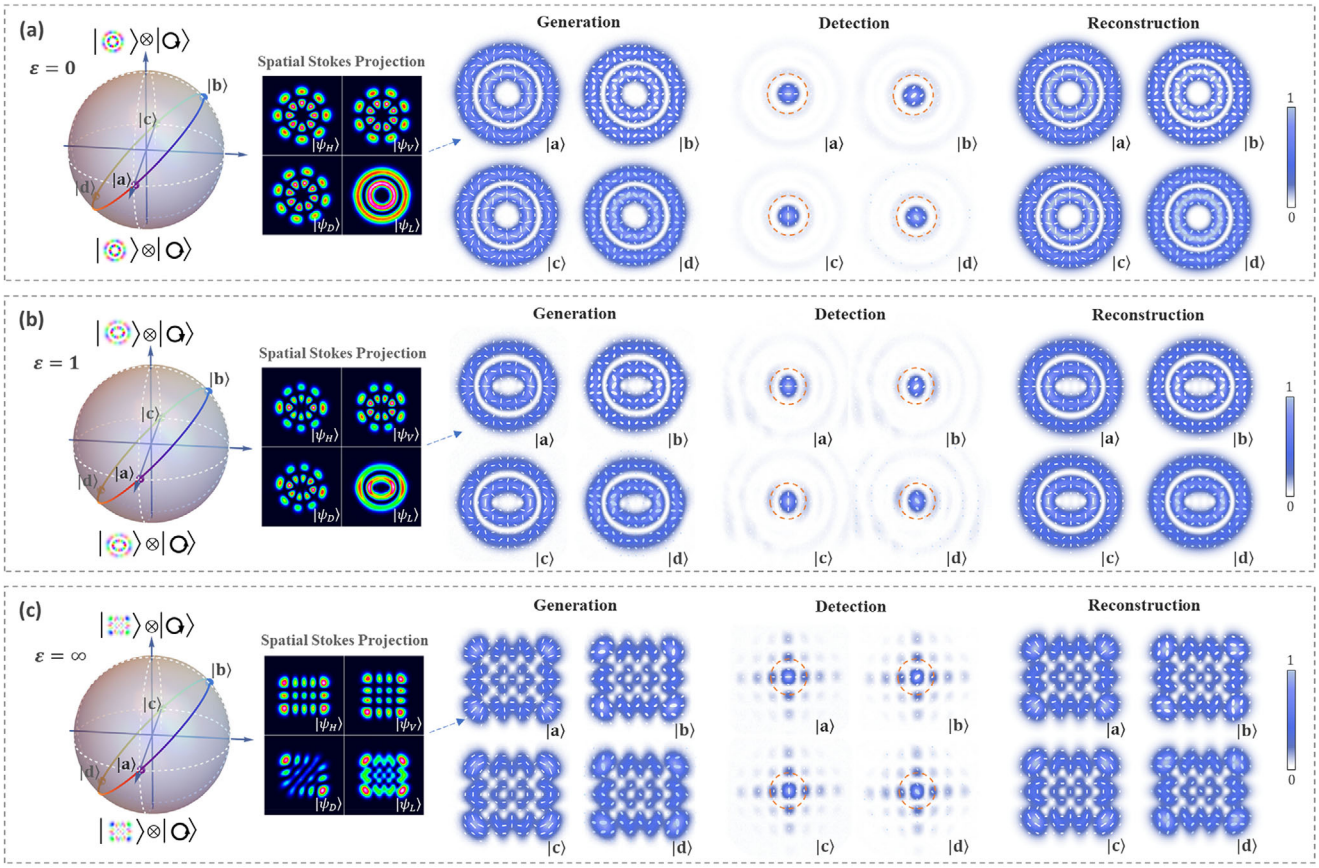

Figure 3. Experimental results of the reciprocal SOC conversion used for the generation and detection of generalized SOC modes, where a–c) correspond to vector IG modes with $\varepsilon = 0,\ 1,$ and ∞, respectively. In the detection column, only the SoPs covering on the center patterns surrounded by orange dashed circles were coupled into the SMF and used to determine SOC states. Additional data acquired by spatial Stokes measurement are provided in the Supporting Information.

In the experiment, to show the modal versatility of the principle (i.e., generate and measure arbitrary spatial modes), SGPGs were designed to control a group of generalized SOC states in elliptical coordinates, that is, vector Ince-Gauss (IG) modes.[37] As vector eigen solutions of the paraxial wave equation, they have a propagation-invariant beam structure but, unlike the CV mode, are usually not rotationally symmetric. This indicates that the helical mode pair $\psi_{\pm}(r, z)$ within the "generalized" SOC state probably does not carry well-defined OAMs per photon. Specifically, here, helical IG modes $\mathrm{IG}^{\pm}_{6,4} = \sqrt{1/2}\ (\mathrm{IG}^{e}_{6,4} \pm i\mathrm{IG}^{o}_{6,4})$ with three ellipticities $\varepsilon = 0,\ 1$ and ∞ (see Supporting Information) were chosen for $\psi_{\pm}(r, z)$, corresponding to a transition from $\mathrm{LG}_{\pm 4,1}$ to $\mathrm{IG}^{\pm}_{6,4}$ and finally to helical Hermite–Gauss (HG) modes $\sqrt{1/2}(\mathrm{HG}_{42} \pm i\mathrm{HG}_{33})$. Figure 2b shows the designed LC director distributions (left) and observed polarizing micrographs (middle) of the SGPGs used in experiments, as well as their spin-switchable geometric phase and corresponding complex amplitudes to be structured (right) in theory. In all three cases, it was seen that the structured complex amplitude conjugates had the same intensity profile but opposite OAMs; so, each pair could form an SU(2) unit sphere regarding the OAM. In particular, the average OAMs per photon carried by the helical IG ($\pm 3.89\hbar$) and HG ($\pm 3.46\hbar$) modes were calculated by reconstructing them with superposition of LG modes with the same order $N = 2p + |\ell| = 6$.[54,55] See Supporting Information for details on the paraxial Gaussian modes.

The experimental results are shown in **Figure 3**. For each ellipticity, four states were chosen, evenly spaced on the rainbow-colored circle on the higher-order Poincaré sphere, as desired SOC states to be generated and measured. The polarizing beam patterns shown in the first (Generation) column were experimentally generated vector modes that the authors observed using spatial Stokes polarimetry. As an example, black insets nearby the Generation column show the observed spatial Stokes projection of each state |a⟩. It was seen that the effect of the SOC state transition from state |a⟩ to |d⟩, or the motion on the higher-order Poincaré sphere, was reflected in the variation of SoP distributions. The position parameters, that is, a and θ, according to Equation (3), could be measured quantitatively by converting the vector mode back into the corresponding scalar one. The middle (Detection) column shows the observed polarizing beam patterns sampled from the NPBS after detection by SOC-II. The theory regarding the pattern evolution in vector mode detection is given in the Supporting Information. Here, only the central Gaussian-like patterns were coupled into the SMF, and SoPs covering them were used to determine the position parameters a and θ, as

indicated by the colored dots embedded on the rainbow path to show the measured positions. For a more intuitive comparison, the right (Reconstruction) column shows the simulated polarizing beam pattern of each involved SOC state according to the measured position parameters. That is, these patterns were calculated via Equation (1) with specific $\psi_{\pm}(\boldsymbol{r}, z)$ and using measured a and θ as input. The theoretical reconstruction was shown to be highly consistent with that in the observation, verifying the precision of the device in both SOC state generation and detection.

4. Conclusion and Discussion

We experimentally demonstrated a new type of photonic SOC device, the SGPG, using the LC geometric phase. This advanced SOC device, compared with the present generation of devices, such as the q-plate, enables conjugate complex-amplitude control of orthogonal circular polarizations by bringing in a spatially varied grating microstructure. Such a crucial advance unlocks the control of paraxial structured light in all spatial dimensions via geometric phase. Taking the results in Figure 3a as an example, the accession of radial modes further boosts the dimensions (or data capacity) of a quantum (or spatial-division multiplex) system relative to those of a photonic SOC system controlled by q-plates. In addition to the special CV modes, as shown in Figure 3b,c, the device can control generalized SOC states without rotational symmetry (or well-defined OAM). This capability makes it a key extra-/intracavity component to build a structured laser that has greater tunability in beam structure, compared with reported systems based on q-plate and metasurface.[56,57] For quantum optics, the reciprocal SOC interface demonstrated here allows to implement a Bell measurement for arbitrary SOC states, which is the basis toward the teleportation scheme for SOC photon pairs.[46] Moreover, owing to the capability of full-field spatial mode control,[39] the device also paves the way to quantum control of high-dimension photonic skyrmions.[58,59]

Beyond single-beam vector mode control, this principle can further realize multiple vector mode control through the addition of a Dammann grating structure;[12,60,61] see Supporting Information for an extended discussion. This represents a promising way to develop information exchange and processing units working for photonic SOC states, that is, vector-mode multiplexers and demultiplexers. Moreover, the existence of the grating phase makes the diffraction response tunable with both the polarization and temporal spectrum of the incident beam, suggesting that the principle may also be used to shape and control the nonseparable structure of paraxial light in ray-wave coupled and spatiotemporal degrees of freedom.[62–67] Another issue of concern is the fabrication complexity, and another key advantage of SGPG is that it only requires the birefringence microstructure having a spatially varied orientation with global identical retardation, that is, the complexity is same as the fabrication of q-plates. Hence, this new-type SOC device can be easily commercially manufactured, especially the LC version enabled by the photoalignment technique.

Regarding the limitation of the SOC device presented here; although, the key LC element SGPG supports arbitrary complex-amplitude control with SoP switchable behaviour, the crucial amplitude control is realized by introducing spatially-varying grating; as a consequence, the generated or measured mode conjugates $\psi_{\pm}(\boldsymbol{r}, z)$ are separated to $\pm$1st-order diffractions. Such spatial separation of $\psi_{\pm}(\boldsymbol{r}, z)$ is useful for the applications that require shaping arbitrary scalar mode with SoP switchable behaviour. For vector mode control; however, we have to use a 4*f*-PG system with the phase-locking capacity to recombine the spatially separated $\psi_{\pm}(\boldsymbol{r}, z)$, leading to the whole SOC device bulky. To further simplify the components of the device, in principle, the 4*f* lens can also be replaced by geometric phase elements. However, for single-beam vector mode control, reciprocal SOC conversion realized via a single flat element is preferred; and thus, is still a worthy issue to further research.

5. Methods

5.1. LC Microstructure Fabrication

The sulfonic azo-dye SD1 (Dai-Nippon Ink and Chemicals, Japan) was dissolved in dimethylformamide at a concentration of 0.3 wt% and used as the photoalignment agent. Two indium-tin-oxide glasses were ultrasonic and UV-ozone cleaned. After that, they were spin-coated with the SD1 solution at 800 rpm for 10 s, and then, at 3000 rpm for 40 s. After curing at 100 °C for 10 min, the two glasses were assembled into a 6-μm-thick empty cell with the aid of spacers. Next, a digital-micromirror-device (DMD) based photoalignment system was used to fulfill the dynamic multi-step photoalignment process.[68] The DMD (Discovery 3000, Texas Instruments) consisted of 1024 × 768 micromirrors with the pixel size of 13.68 μm × 13.68 μm, and a 5× objective was used to further reduce the pixel pitch. When loading the designed alignment patterns, this system exposed the cell to UV light in a multi-step manner with a total dose of ≈5 J cm^{-2}. Each step corresponded to a specific exposure pattern and a certain UV linear polarization direction. As SD1 molecules tend to reorient perpendicular to the UV polarization direction, the SD1 layers could be endowed with the desired alignment distribution after photoalignment process. Last, the nematic LC E7 (HCCH, China) was filled into the cell at 70 °C via the capillary action. After cooling to room temperature, the LC molecules acquired the same director distribution as SD1 through intermolecular interactions.

Supporting Information

Supporting Information is available from the Wiley Online Library or from the author.

Acknowledgements

C.-Y.L. and S.-J.L. contributed equally to this work. This work was supported by the National Natural Science Foundation of China (Grant Nos. 62075050, 62222507, 11934013, 61975047, 12004175, and 62175101), the Innovation Program for Quantum Science and Technology (No. 2021ZD0301500), and the Natural Science Foundation of Jiangsu Province (Nos. BK20212004 and BK20200311)

Conflict of Interest

The authors declare no conflict of interest.

Data Availability Statement

The data that support the findings of this study are available from the corresponding author upon reasonable request.

Keywords

flat-optics, geometric phase, liquid-crystal, spin-orbit coupling

Received: October 21, 2022
Revised: January 17, 2023
Published online: February 8, 2023

[1] H. Rubinsztein-Dunlop, A. Forbes, M. V. Berry, M. R. Dennis, D. L. Andrews, M. Mansuripur, C. Denz, C. Alpmann, P. Banzer, T. Bauer, E. Karimi, L. Marrucci, M. Padgett, M. Ritsch-Marte, N. M. Litchinitser, N. P. Bigelow, C. Rosales-Guzmán, A. Belmonte, J. P. Torres, T. W. Neely, M. Baker, R. Gordon, A. B. Stilgoe, J. Romero, A. G. White, R. Fickler, A. E. Willner, G. Xie, B. Mcmorran, A. M. Weiner, *J. Opt.* **2016**, *19*, 013001.
[2] J. Chen, C. Wan, Q. Zhan, *Sci. Bull.* **2018**, *63*, 54.
[3] J. Wang, F. Castellucci, S. Franke-Arnold, *AVS Quantum Sci.* **2020**, *2*, 031702.
[4] A. Forbes, M. De Oliveira, M. R. Dennis, *Nat. Photonics* **2021**, *15*, 253.
[5] D. Pohl, *Appl. Phys. Lett.* **1972**, *20*, 266.
[6] L. Allen, M. W. Beijersbergen, R. J. C. Spreeuw, J. P. Woerdman, *Phys. Rev. A* **1992**, *45*, 8185.
[7] Y. Shen, X. Wang, Z. Xie, C. Min, X. Fu, Q. Liu, M. Gong, X. Yuan, *Light: Sci. Appl.* **2019**, *8*, 90.
[8] K. Y. Bliokh, F. J. Rodríguez-Fortuño, F. Nori, A. V. Zayats, *Nat. Photonics* **2015**, *9*, 796.
[9] V. S. Liberman, B. Y. Zel'dovich, *Phys. Rev. A* **1992**, *46*, 5199.
[10] C. V. S. Borges, M. Hor-Meyll, J. A. O. Huguenin, A. Z. Khoury, *Phys. Rev. A* **2010**, *82*, 033833.
[11] C. Rosales-Guzmán, B. Ndagano, A. Forbes, *J. Opt.* **2018**, *20*, 123001.
[12] C. Rosales-Guzmán, A. Forbes, *How to Shape Light With Spatial Light Modulators*, SPIE Press, **2017**.
[13] F. Cardano, L. Marrucci, *Nat. Photonics* **2015**, *9*, 776.
[14] A. H. Dorrah, F. Capasso, *Science* **2022**, *376*, eabi6860.
[15] P. Chen, B. Y. Wei, W. Hu, Y. Q. Lu, *Adv. Mater.* **2020**, *32*, 1903665.
[16] C. Cisowski, J. Götte, S. Franke-Arnold, *Rev. Mod. Phys.* **2022**, *94*, 031001.
[17] E. Cohen, H. Larocque, F. Bouchard, F. Nejadsattari, Y. Gefen, E. Karimi, *Nat. Rev. Phys.* **2019**, *1*, 437.
[18] S. Pancharatnam, 1956-Proceedings of the Indian Academy of Sciences-Section A.
[19] R. C. Devlin, A. Ambrosio, N. A. Rubin, J. P. B. Mueller, F. Capasso, *Science* **2017**, *358*, 896.
[20] L. Marrucci, C. Manzo, D. Paparo, *Phys. Rev. Lett.* **2006**, *96*, 163905.
[21] Q. Zhan, *Adv. Opt. Photonics* **2009**, *1*, 1.
[22] E. Nagali, L. Sansoni, L. Marrucci, E. Santamato, F. Sciarrino, *Phys. Rev. A* **2010**, *81*, 052317.
[23] Z. Zhuo-Dan, Z. Shang-Hong, D. Chen, S. Ying, *Phys. Rev. A* **2008**, *65*, 1529.
[24] R. Dorn, S. Quabis, G. Leuchs, *Phys. Rev. Lett.* **2003**, *91*, 233901.
[25] G. Vallone, V. D'ambrosio, A. Sponselli, S. Slussarenko, L. Marrucci, F. Sciarrino, P. Villoresi, *Phys. Rev. Lett.* **2014**, *113*, 060503.
[26] A. Sit, F. Bouchard, R. Fickler, J. Gagnon-Bischoff, H. Larocque, K. Heshami, D. Elser, C. Peuntinger, K. Günthner, B. Heim, C. Marquardt, G. Leuchs, R. W. Boyd, E. Karimi, *Optica* **2017**, *4*, 1006.
[27] B. Ndagano, B. Perez-Garcia, F. S. Roux, M. Mclaren, C. Rosales-Guzman, Y. Zhang, O. Mouane, R. I. Hernandez-Aranda, T. Konrad, A. Forbes, *Nat. Phys.* **2017**, *13*, 397.
[28] V. D'ambrosio, N. Spagnolo, L. Del Re, S. Slussarenko, Y. Li, L. C. Kwek, L. Marrucci, S. P. Walborn, L. Aolita, F. Sciarrino, *Nat. Commun.* **2013**, *4*, 2432.
[29] E. Karimi, G. Zito, B. Piccirillo, L. Marrucci, E. Santamato, *Opt. Lett.* **2007**, *32*, 3053.
[30] Z. Y. Zhou, Z. H. Zhu, S. L. Liu, Y. H. Li, S. Shi, D. S. Ding, L. X. Chen, W. Gao, G. C. Guo, B. S. Shi, *Sci. Bull.* **2017**, *62*, 1185.
[31] E. Karimi, R. W. Boyd, P. De La Hoz, H. De Guise, J. Řeháček, Z. Hradil, A. Aiello, G. Leuchs, L. L. Sánchez-Soto, *Phys. Rev. A* **2014**, *89*, 063813.
[32] E. Karimi, D. Giovannini, E. Bolduc, N. Bent, F. M. Miatto, M. J. Padgett, R. W. Boyd, *Phys. Rev. A* **2014**, *89*, 013829.
[33] Y. Zhang, F. S. Roux, M. Mclaren, A. Forbes, *Phys. Rev. A* **2014**, *89*, 043820.
[34] V. D. Salakhutdinov, E. R. Eliel, W. Löffler, *Phys. Rev. Lett.* **2012**, *108*, 173604.
[35] L. Chen, T. Ma, X. Qiu, D. Zhang, W. Zhang, R. W. Boyd, *Phys. Rev. Lett.* **2019**, *123*, 060403.
[36] R. Y. Zhong, Z. H. Zhu, H. J. Wu, C. Rosales-Guzmán, S. W. Song, B. S. Shi, *Phys. Rev. A* **2021**, *103*, 9.
[37] Y. Li, X. B. Hu, B. Perez-Garcia, B. Zhao, W. Gao, Z. H. Zhu, C. Rosales-Guzmán, *Appl. Phys. Lett.* **2020**, *116*, 221105.
[38] M. A. Bandres, J. C. Gutiérrez-Vega, *Opt. Lett.* **2004**, *29*, 144.
[39] F. Brandt, M. Hiekkamäki, F. Bouchard, M. Huber, R. Fickler, *Optica* **2020**, *7*, 98.
[40] H. J. Wu, B. S. Yu, Z. H. Zhu, W. Gao, D. S. Ding, Z. Y. Zhou, X. P. Hu, C. Rosales-Guzman, Y. Shen, B. S. Shi, *Optica* **2022**, *9*, 187.
[41] D. Sugic, R. Droop, E. Otte, D. Ehrmanntraut, F. Nori, J. Ruostekoski, C. Denz, M. R. Dennis, *Nat. Commun.* **2021**, *12*, 6785.
[42] B. P. Da Silva, V. A. Pinillos, D. S. Tasca, L. E. Oxman, A. Z. Khoury, *Phys. Rev. Lett.* **2020**, *124*, 033902.
[43] L. J. Pereira, A. Z. Khoury, K. Dechoum, *Phys. Rev. A* **2014**, *90*, 053842.
[44] G. Milione, H. I. Sztul, D. A. Nolan, R. R. Alfano, *Phys. Rev. Lett.* **2011**, *107*, 053601.
[45] R. Gutiérrez-Cuevas, S. Wadood, A. N. Vamivakas, M. A. Alonso, *Phys. Rev. Lett.* **2020**, *125*, 123903.
[46] A. Z. Khoury, P. Milman, *Phys. Rev. A* **2011**, *83*, 060301.
[47] P. Chen, L. L. Ma, W. Duan, J.i Chen, S. J. Ge, Z. H. Zhu, M. J. Tang, R. Xu, W. Gao, T. Li, W. Hu, Y. Q. Lu, *Adv. Mater.* **2018**, *30*, 1705865.
[48] P. Chen, Z. X. Shen, C. T. Xu, Y. H. Zhang, S. J. Ge, L. L. Ma, W. Hu, Y. Q. Lu, *Laser Photonics Rev.* **2022**, *16*, 2200011.
[49] P. Chen, L. L. Ma, W. Hu, Z. X. Shen, H. K. Bisoyi, S. B. Wu, S. J. Ge, Q. Li, Y. Q. Lu, *Nat. Commun.* **2019**, *10*, 2518.
[50] L. Zhu, C. T. Xu, P. Chen, Y.-H. Zhang, S.-J. Liu, Q.-M. Chen, S.-J. Ge, W. Hu, Y.-Q. Lu, *Light: Sci. Appl.* **2022**, *11*, 135.
[51] E. Toninelli, B. Ndagano, A. Vallés, B. Sephton, I. Nape, A. Ambrosio, F. Capasso, M. J. Padgett, A. Forbes, *Adv. Opt. Photonics* **2019**, *11*, 67.
[52] B. Ndagano, I. Nape, M. A. Cox, C. Rosales-Guzman, A. Forbes, *J. Lightwave Technol.* **2018**, *36*, 292.
[53] B. S. Yu, C. Y. Li, Y. Yang, C. Rosales-Guzmán, Z. H. Zhu, *Laser Photonics Rev.* **2022**, *16*, 2200260.
[54] H. R. Yang, H. J. Wu, W. Gao, C. Rosales-Guzmán, Z. H. Zhu, *Opt. Lett.* **2020**, *45*, 3034.
[55] W. N. Plick, M. Krenn, R. Fickler, S. Ramelow, A. Zeilinger, *Phys. Rev. A* **2013**, *87*, 033806.
[56] H. Sroor, Y. W. Huang, B. Sephton, D. Naidoo, A. Vallés, V. Ginis, C. W. Qiu, A. Ambrosio, F. Capasso, A. Forbes, *Nat. Photonics* **2020**, *14*, 498.
[57] D. Naidoo, F. S. Roux, A. Dudley, I. Litvin, B. Piccirillo, L. Marrucci, A. Forbes, *Nat. Photonics* **2016**, *10*, 327.

[58] Y. Shen, B. Yu, H. Wu, C. Li, Z. Zhu, A. V. Zayats, *Adv. Photonics* **2023**, *5*, 015001.
[59] D. Sugic, R. Droop, E. Otte, D. Ehrmanntraut, F. Nori, J. Ruostekoski, C. Denz, M. R. Dennis, *Nat. Commun.* **2021**, *12*, 6785.
[60] P. Chen, S. J. Ge, W. Duan, B. Y. Wei, G. X. Cui, W. Hu, Y. Q. Lu, *ACS Photonics* **2017**, *4*, 1333.
[61] S. Liu, P. Chen, S. Ge, L. Zhu, Y. H. Zhang, Y. Q. Lu, *Laser Photonics Rev.* **2022**, *16*, 2200118.
[62] Y. Shen, C. Rosales-Guzmán, *Sci. Rep.* **2016**, *6*, 25528.
[63] C. He, Y. Shen, A. Forbes, *Light: Sci. Appl.* **2022**, *11*, 205.
[64] Y. Shen, X. Yang, D. Naidoo, X. Fu, A. Forbes, *Optica* **2020**, *7*, 820.
[65] Y. Shen, I. Nape, X. Yang, X. Fu, M. Gong, D. Naidoo, A. Forbes, *Optica* **2021**, *10*, 10.
[66] C. Wan, Q. Cao, J. Chen, A. Chong, Q. Zhan, *Nat. Photonics* **2022**, *16*, 519.
[67] C. Wan, J. Chen, A. Chong, Q. Zhan, *Natl. Sci. Rev.* **2022**, *9*, 149.
[68] W. Ji, C. H. Lee, P. Chen, W. Hu, Y. Ming, L. Zhang, T. H. Lin, V. Chigrinov, Y. Q. Lu, *Sci. Rep.* **2016**, *6*, 25528.